Indian Journal of Radio & Space Physics
Vol. 31, August 2002, pp. 183-189

Numerical simulation of magnetic reconnection and plasmoid dynamics in the geotail

Manashi Roy & G S Lakhina

Indian Institue of Geomagnetism Colaba, Mumbai 400 005

Received 16 August 2001; revised 26 November 2001; accepted 14 February 2002

The time evolution of the geotail is represented by a set of single fluid magnetohydrodynamic (MHD) equations. The initial equilibrium is allowed to be destroyed by a finite, but very small electric resistivity, so that the fluid is still an almost ideal MHD system. The subsequent evolution of the geotail is investigated by a two-dimensional numerical code. The onset of reconnection and formation of magnetic island-like structures called plasmoids are reproduced. The velocity pattern and the size of plasmoid are investigated under different initial conditions and are compared with actual observations in space.

1 Introduction

The interaction of solar wind and the geomagnetic field produces a current system across the central plasma sheet at the nightside of the distant magnetosphere called the geotail. Increased solar wind velocity and magnetic field result in the intensification of these dawn-dusk currents in the geotail which results in the stretching of the magnetic field lines along the tail axis. Although the earth-ward ends of the tail fields are dipole-like field lines, the tail fields become almost parallel to the tail axis at the far end of the tail. This type of field configuration is unstable under various types of magnetohydrodynamic (MHD) instabilities leading to the onset of the reconnection processes. Actually it is this reconnection process which is, among others, an efficient way for the solar wind energy to enter the magnetosphere. Reconnection can be induced by various plasma processes. Although the tearing mode is considered to be the main candidate to induce collisionless reconnection, there are suggestions by Uberoi *et al.*[1,2] that long wavelength surface waves or Alfven resonances[3] also can induce magnetic reconnection leading to the transfer of energy from the solar wind to the magnetosphere. The plasma which was considered to be a perfectly conducting fluid initially acquires a finite resistivity. This, in turn, causes almost anti-parallel magnetic field lines near the tail axis to be reconnected and attains a different topological configuration. Closed magnetic islands are formed[4-6] which are transported tail-ward at a fast rate. Geomagnetic substorm is thought to be initiated by the reconnection process at the near-earth end of the geotail.

Large-scale plasmoid structures propagating at high speed down-tail away from the earth have been observed by several workers[4,7]. The formation and subsequent tail-ward motion of the plasmoids can be explained in the framework of the near-earth neutral line (NENL) model as proposed by Schindler[8] and later by Hones[9] in seventies. According to this model, a neutral line is formed near the tail region as a result of the onset of magnetic reconnection as mentioned earlier, and a part of the stored magnetic energy is converted into particle energy. Plasma and magnetic flux are transported earth-ward and tail-ward. Since the earth-ward plasma flow and the diversion of the tail currents into field-aligned currents are the signatures of the substorms, we term this onset of reconnection as the onset of the substorm itself.

These phenomena have been investigated both analytically and by numerical simulation by a large number of workers[10-15] in the past, who employed different numerical techniques with different initial configuration or different resistivity models. The idea has been to investigate many possible configurations to understand the inherent physics as well as the observational results.

Essentially each numerical code handles the MHD equations slightly differently. Apart from the set of equations being mutually coupled, the problem is further compounded by the inherent non-linear structure of the equations which tend to amplify small differences over the time. Therefore, there had been a need for such numerical experimentation with different code which was realised in the past[14]. Most of these workers[5,6,10,12,14-16] have used one of the two different codes, namely, modified explicit leapfrog

scheme and/or FLIP-MHD scheme. While the flux corrected transport (FCT) code has been successfully applied to other geophysical plasma phenomena, geotail plasma dynamics have not been studied previously using this code.

The purpose of the present study is to employ a FCT scheme to study magnetotail dynamics under different initial conditions. This code is specially suitable for situations where there is a sharp spatial change in the parameters. Since shock-like structures are known to be created at the geotail during the substorm growth and expansion phases, it is felt that the FCT code will be rather appropriate to investigate the evolution of the geotail under the influence of finite resistivity.

2 Governing equations and the initial configurations

The plasma in Cartesian geometry obeys the following compressible, time-dependent resistive equations:

$$\partial\rho/\partial t + \nabla.(\rho\mathbf{V}) = 0 \qquad \ldots (1)$$

$$\partial(\rho\mathbf{V})/\partial t + \mathbf{V}.\nabla(\rho\mathbf{V}) = -\nabla p + \nabla\times\mathbf{B}\times\mathbf{B} \qquad \ldots (2)$$

$$\partial\mathbf{B}/\partial t = \nabla\times(\mathbf{V}\times\mathbf{B}) - \nabla\times(\eta\nabla\times\mathbf{B}) \qquad \ldots (3)$$

$$\partial e/\partial t + \nabla.(e\mathbf{V}) = -p\nabla.\mathbf{V} + \eta^2(\nabla\times\mathbf{B})^2 \qquad \ldots (4)$$

$$\nabla\cdot\mathbf{B} = 0. \qquad \ldots (5)$$

The energy variable e is defined by $e = p/(\gamma-1)$, where γ is the ratio of the two specific heats. The other variables have the usual meanings. We have assumed the resistivity η to be constant, although some workers have assumed η as a function of the current density j.

The simulation region is a two-dimensional box with the x-axis pointing towards the earth and the z-axis to the normal of the current sheet. Variables are assumed to have no variation along the y-direction. The earth-end origin at $x = 0$ is an arbitrary point several earth radii away from the surface of the earth. For the spatial co-ordinate we have chosen the earth's radius R_e as the unit. The units of the density and the magnetic field are chosen as some constants ρ_0 and B_0, respectively, the values of which will be adjusted later. The unit of the velocity is chosen to be the Alfven velocity, V_A, defined by the above constants. The unit of time t is chosen as R_e/V_A. All the variables and parameters are thus dimensionless numbers. For a typical central plasma sheet, V_A is of the order of 1200 km/s.

The model is treated as an initial and boundary value problem. Initially, the plasma is in static equilibrium with geomagnetic field. The tail configuration of the geomagnetic field is generally represented[15] by a vector potential with y-component

$$a_y \propto \log\left(\cosh\left(\frac{z}{f}\right)\right) + \log(f)$$

The magnetic field and the currents are given by

$\mathbf{B} = B_0\nabla\times\mathbf{a}_y$ and

$\mathbf{j} = \nabla\times\mathbf{B}$, respectively,

where, f is a function of only x and represents the width of the current sheet at x in dimensionless unit. The x variation of the function f tells us as to how stretched the magnetic field lines are. Generally, a weak variation of the form[12,15]: $f = f_0.(1-\alpha.x)^{0.5}$ represents a reasonable tail field.

The density is assumed to be equal to pressure at $t = 0$. The initial velocity is also assumed to be zero at all points in space. The magnetic field is normalized so that B_x at $z = z_{max}$ is unity. Similarly the density ρ is normalized by its value at $z = 0$, $x = x_{max}$, i.e. at the earth-end of the simulation box on the z-axis. The initial pressure profile is calculated by putting the L.H.S. of Eq. (2) to zero and integrating the magnetic fields.

The subsequent time evolution is obtained by integrating the MHD equations numerically. A flux-corrected transport code (FCT) has been applied here to solve this set of equations.

The FCT code was originally conceived by DeVore[17] and has been developed over the years as a method for accurately solving the conservation equations of hydrodynamics without violating the positivity of mass and energy, particularly, near shocks and other discontinuities (Ref. 17 and references therein). This is achieved by adding to the equations a strong numerical diffusion, which guarantees the positivity. The error introduced by this diffusion term is kept minimum by introducing an anti-diffusion term in the next stage. It also ensures that the divergence of the magnetic field is zero all the time.

The boundary conditions are as follows:

At the earth-end of the simulation box ($x = x_{max}$) the velocity is zero, $\partial\rho/\partial x = 0$; $\partial p/\partial x = 0$ and $\partial B_z/\partial x = 0$. We have assumed the variation of the velocity components with respect to x to vanish at the tail-ward side of the simulation box which makes it a free boundary. At the top and bottom boundaries, i.e. at $z = z_{max}$ and at $z = z_{min}$, we have taken $\partial V_x/\partial z = 0$; $\partial B_x/\partial z = 0$; $\partial\rho/\partial z = 0$; and $\partial p/\partial z = 0$. The other components of the **B** field are adjusted to make divergence of **B** vanish at the boundary.

3 Results and discussion

The time evolution of the magnetic field configurations are shown in Fig. 1 for a narrow current width with $f_0 = 1.22$. The reconnection sets in after $t = T_c = 100$ units. The X-type neutral point is formed very close to the earth-end of the simulation box at $x = -4$. It is also accompanied by another neutral point, called the O-point slightly tail-ward, thereby creating a small magnetic closed island. This smallest plasmoid is formed almost immediately, very close to the neutral X-point. The centre of the plasmoid, which is the neutral O-point, moves tail-ward. Actually both the neutral points move tail-ward, the latter more rapidly than the former. As a result, the separation between the two neutral points increases with time. The position of the O-point as a function of time is plotted in Fig. 2, where the results are presented for three sets of runs for three different values for the current widths $f_0 = \sqrt{1.5} = 1.22$; $f_0 = \sqrt{2} = 1.41$ and $f_0 = \sqrt{3} = 1.73$, respectively. The reconnection time T_c increases with the increase of the current width. In Fig. 2 time is measured relative to the respective reconnection time T_c. Initially, the rate at which the O-point shifts tail-ward does not seem to depend much on the width of the current sheet.

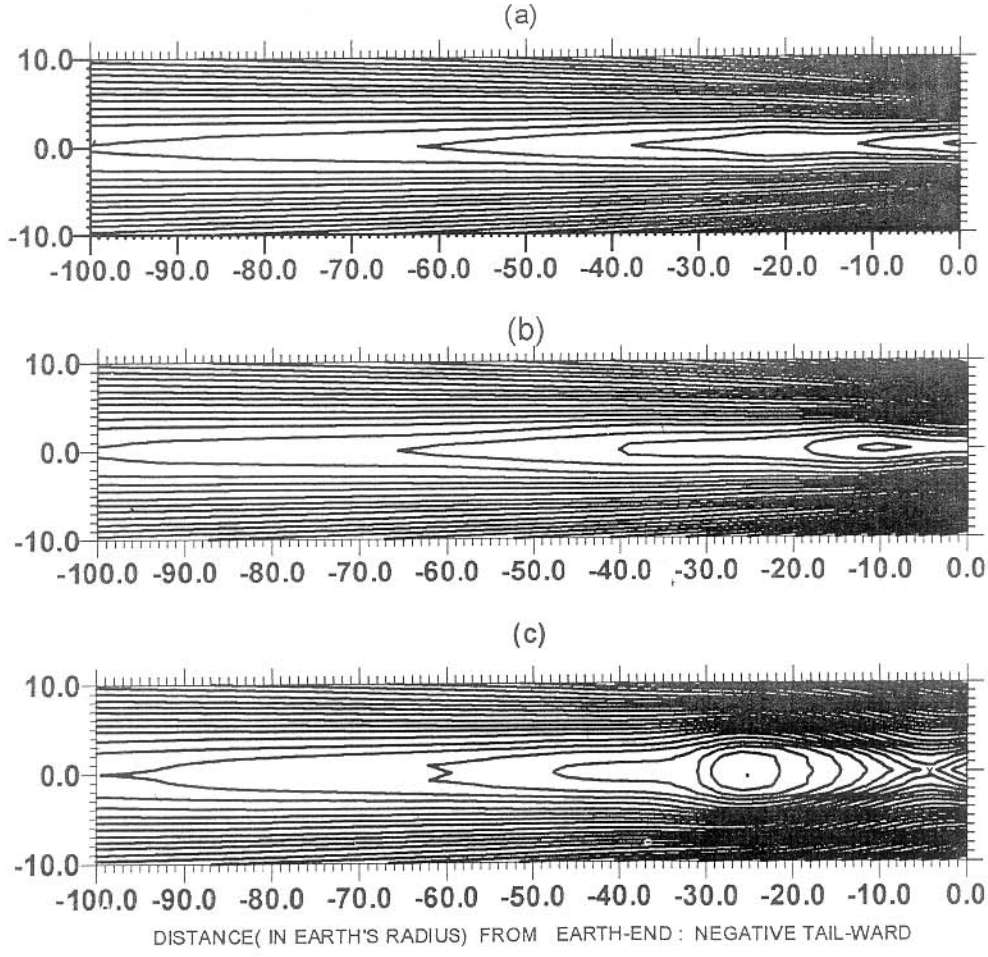

Fig. 1—Time evolution of the magnetic field configuration in the x-z plane [The reconnection starts at $t = T_c$. The pattern of the field lines at (a) 5 units of time before T_c, (b) 25 units of time after T_c, (c) 75 units of time after T_c. The width f_0 of the initial current sheet is 1.22. The centre of the plasmoid (neutral point O) and the X-point (site of reconnection) are labelled by the letter O and by a dot, respectively, in the diagram (c).]

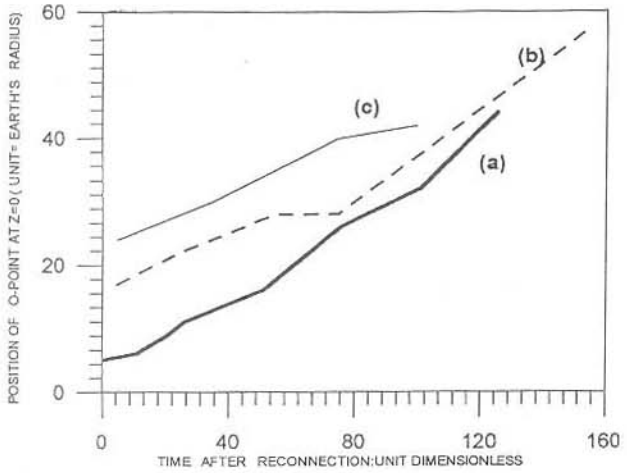

Fig. 2—Position of the neutral O-point on the x-axis as a function of time measured from T_c, the onset of reconnection, for three current widths (a) 1.22, (b) 1.41 and (c) 1.73

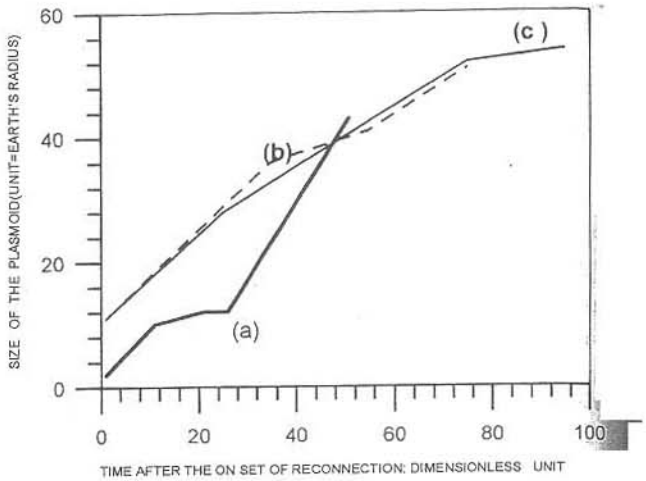

Fig. 3—Size of the plasmoid along the x-axis as a function of time for current widths (a) 1.22, (b) 1.41 and (c) 1.73

However, at the later time the thinner current sheet [case (a)] seems to imply a slightly faster tail-ward motion of the O-point.

The size of the plasmoid may be defined to be the area between the last closed field line near the X-point, i.e. the area closed by the separatrix. This size will be relevant only if the whole area, as defined, is within the simulation box. As the plasmoid grows in size the tail end of the separatrix goes beyond the simulation box and, therefore, plasmoid size is undefined. In Fig. 3, the plasmoid size has been plotted as a function of time t for the current widths (a) 1.22, (b) 1.41, and (c) 1.73. Because of the above mentioned difficulty the plasmoid size could be estimated only up to a limited time.

The plasmoid size is initially much smaller for case (a) in Fig. 3 which has the thinnest current sheet. In this case it first grows slowly, and after about 25 units of time it suddenly grows at a much faster rate. In contrast, the plasmoid sizes grow at slower rates throughout the duration of the simulation for the wider current widths. Because of the onset of numerical noise, it was not possible to continue the simulation further and sizes of these magnetic islands could not be estimated. The wider current width means that the field lines were less stretched at $t = 0$. Thus, the size as well as the growth rate of the plasmoid are seen to depend on how much the magnetic field lines are stretched before the resistivity is introduced at $t = 0$.

The observational values of the plasmoid sizes exhibit a large variation depending on the location of the satellite and the individual substorms. Scholer *et al.*[18] estimated typical lengths to be between 50 and 100 R_e when the locations of the satellite ISEE-3 were at distances between 110 and 220 R_e. On the other hand, the observation of Moldwin and Hughes[7] estimates a much smaller size of 16 ± 13 R_e. Similarly Haland *et al.*[19] also observed the plasmoid sizes to be less than 10 R_e at the near-earth regions. For such a small-sized plasmpoid structure the initial current width has to be rather narrow and of the order of one earth-radius as inferred from the present simulation results. The present numerical experiments also suggest that the plasmoid size is very small at the initial stages of its formation when the structure is confined at the earth-end side. As the structure moves tail-ward, its size increases and can be of the order of a few tens of R_e at the mid- and far end of the tail. Therefore, it is rather natural that the observed sizes of plasmoids show such a large variation.

In the present simulation model the plasmoids are two-dimensional structures. In contrast to the size along x-direction, its z-directional extent is much smaller. Since the system is symmetric about $z = 0$, the actual size in z-direction is twice the half size. In case of the thinnest current width [case (a) in Fig. 3], this half size along the z-direction grows from about 1 R_e at $t = +0$ to about 4.8 R_e at 200 units of time after the onset of reconnection. For the other two cases, sizes along the z-direction are slightly larger. This is only to be expected, as the initial field configurations are broader for the wider current widths. Thus, the plasmoid is a two-dimensional structure for a very short while immediately after the onset of the reconnection, and then it assumes an essentially x-directional structure.

We have assumed the initial velocity to be zero everywhere at the start of the time integration. As the system evolves with time, the plasma velocity at the central part of the current sheet is predominantly along the x-direction. Therefore, V_x at $z = 0$ (i.e. the flow along the tail-axis in the central plasma sheet) is plotted in Fig. 4 [(a)-(c)] for post-reconnection (t positive relative to T_c) periods. At any instant of time the flow velocity has a spatial variation. The maximum tail-ward velocity V_{max} as a function of time t (measured from reconnection time T_c) is plotted in Fig. 5 for all the three cases.

During the post-reconnection period the plasma flow is negative (i.e. velocity is tail-ward) at the tail-ward locations and positive (velocity earth-ward) at the earth-ward locations with respect to the NENL. On the whole, the tail-ward flow is stronger than the earth-ward flow after the formation of the NENL. Thus, the plasma is ejected in two opposite directions from the NENL location.

The tail-ward flow velocity is different at different locations on the x-axis at any instant of time. At any time the maximum tail-ward velocity, $-V_{max}$, occurs over a finite region on the x-axis. The magnitude of the earth-ward flow velocities also evolve with time. To assess the variation of the flow pattern with current width, we have plotted $-V_{max}$ as a function of time for all the three cases in Fig. 5. The time is measured from the reconnection time T_c. Unlike the plasmoid size, the tail-ward flow is stronger for the narrower current sheet model. The wider the initial current sheet, the weaker is the tail-ward flow after reconnection. In all three cases the flow reaches a maximum and then becomes weaker with time. The initial acceleration of the flow is also stronger for the narrower current sheet [case (a)]. As the position of $-V_{max}$ also shifts tail-ward with time (not shown in Fig. 5), it is reasonable to conclude that the plasma accelerates at a higher rate initially after the onset of the reconnection at the near-tail region. As the plasmoid moves tail-ward the flow rather decelerates. From the observations of a large number of plasmoids Ida *et al.*[20] have concluded that the plasmoids accelerated from 400 km/s to 700 km/s at the near-tail region, but decelerated to about 600 km/s as they travelled to the distant tail. The present simulation results also show the same trend. For the case of narrow current width [case(a)], the plasma flows tail-ward with a velocity of about 0.56, i.e. approximately 670 km/s at $t = 100$ at a location of $x = -25\ R_e$. The unit of velocity is the local Alfven velocity at the

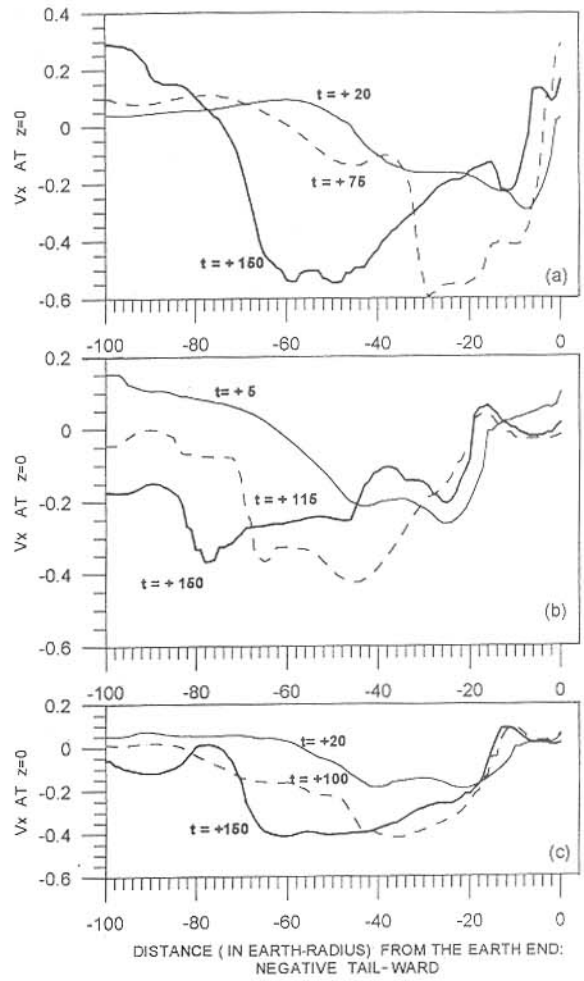

Fig. 4—Tail-ward plasma velocity V_x at $z = 0$, as a function of x at different time t for the three different current widths (a) 1.22, (b) 1.41 and (c) 1.73 [Positive (negative) t means after (before) the reconnection time T_c.]

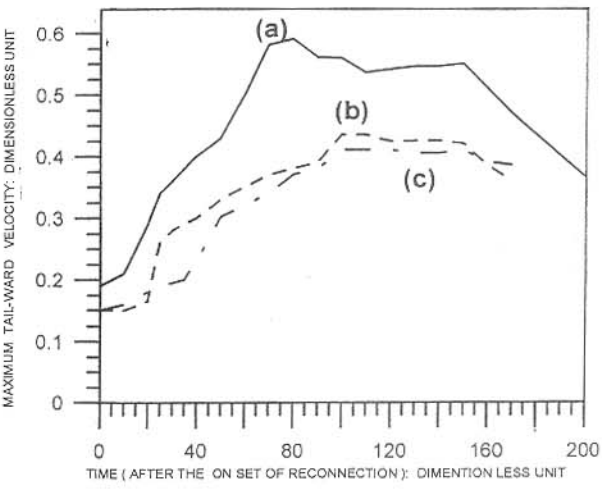

Fig. 5—Maximum tail-ward velocity V_{max} as a function of time for cases (a)-(c) as labelled in Figs 2-4

central plasma sheet which is of the order of 1200 km/s as mentioned earlier. Since the origin is at a distance of about 10 R_e down-tail, this region of −25 R_e amounts to a mid-tail region. The flow velocity at the distant tail of −80 R_e has been reduced to about 0.39 units or about 470 km/s. These numbers are, of course, variables subject to the accuracy of the normalization values for the fields and densities. Nevertheless, the pattern seems to agree with the observations.

One interesting feature of the plasma flow near the reconnection time is that there is a strong earth-ward flow before the onset of the reconnection. In Fig. 6 are plotted the earth-ward velocity V_x at $z = 0$ as a function of distance for two times (relative to T_c) for the runs corresponding to $f_0 = 1.22$. This earth-ward flow peaks in the neighbourhood of the near-earth end, and it shifts slightly tail-ward as the time approaches the onset of the reconnection. The earth-ward plasma flow, before the onset of the reconnection, was observed by Machida *et al.*[21] from statistical analysis of a large number of substorm events. They have concluded that these are the enhanced global convection flow, which are earth-ward. The global convection in response to the increased solar wind speed is known to be the result of reconnection at the distant neutral line (DNL) at the far end of the geotail. This assumes that an earlier reconnection took place at a distant neutral line, before the NENL was formed to initiate the substorm events. However, the present simulation results seem to indicate that earth-ward plasma flow before the onset of reconnection, and hence a substorm, need not originate form DNL reconnection.

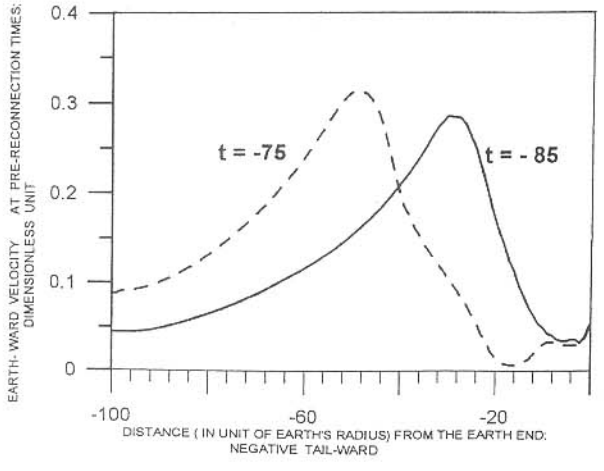

Fig. 6—Earth-ward plasma velocity at $z = 0$ for the thin current width [case (a), i.e. $f_0 = 1.22$] before the onset of the reconnection at T_c

4 Summary and conclusions

The simulation code using the FCT technique to solve the MHD equations with small but finite resistivity reproduces the familiar results of the formation of NENL, a pair of X- and O-points. The field topology changes from dipolar to stretched configuration long before the creation of these neutral points. Subsequently, the onset of magnetic reconnection is accompanied with the formation of closed loops termed plasmoids.

The initial width of the neutral sheet current has a bearing on the time taken for the reconnection to take place after the resistivity is switched on at $t = 0$. The subsequent time evolution of the dynamics of the plasmoid structure are also seen to depend on the initial configuration of the equilibrium state.

The size of the plasmoid is initially found to be rather small (only a few R_e along the x-direction), although it becomes much larger as it moves with a speed of a few hundreds of kilometres per second. An earth-ward plasma flow, before the onset of the substorm as observed by Machida *et al.*[21], can be explained in terms of the fine balance between the time evolution of various plasma parameters involved in the equations. Actually, this earth-ward flow seems to be more consistent with the observations if the initial current width is assumed to be somewhat larger. The flow velocity also increases with time after the onset of the reconnection, and after a while it decreases with time. This variation is rather sluggish, if the initial current width is wider.

References

1 Uberoi C, Lanzerotti L J & Wolfe A, *J Geophys Res (USA)*, 101 (1996) 24979.
2 Uberoi C, Lanzerotti L J & Maclennam C G, *J Geophys Res (USA)*, 104 (1999) 25153.
3 Uberoi C & Zweibel E G, *J Plasma Phys (USA)*, 62 (1999) 345.
4 Richardson I G, Cowley S W H, Hones E W & Bame S J, *J Geophys Res (USA)*, 92 (1987) 9997.
5 Ugai M, *J Geophys Res (USA)*, 90 (1985) 9576.
6 Ugai M, *Phys Fluids B Plasma Phys (USA)*, 1 (1989) 942.
7 Moldwin M B & Hughes W J, *J Geophys Res (USA)*, 97 (1992) 19259.
8 Schindler K, *J Geophys Res (USA)*, 79 (1974) 2803.
9 Hones (Jr) E W, *Physics of Solar Planetary Environments* (AGU, Washington DC, USA), 1976, p. 559.
10 Birn J & Hones (Jr) E W, *J Geophys Res (USA)*, 86 (1981) 6802.
11 Hesse M & Birn J, *J Geophys Res (USA)*, 96 (1991) 5683.
12 Otto A, Schindler K & Birn J, *J Geophys Res (USA)*, 95 (1990) 15023.
13 Pritchett P L & Buchner J, *J Geophys Res (USA)*, 100 (1995) 3601.

14 Birn J, Iinoya F & Brackbill J U, *Geophys Res Lett (USA)*, 23 (1996) 323.

15 Birn J, Michael H & Schindler K, *J Geophys Res (USA)*, 101 (1996) 12939.

16 Otto A, *Reconnection in Space Plasma* (European Space Agency Spec. Publ. SP-285 II), 1988, p. 223.

17 DeVore C R, *Flux-corrected transport algorithm for two-dimensional compressible magnetohydrodynamics* in *NRL Memorandum Report No.6544* (1989).

18 Scholer M, Gloeckler G, Hovestadt D, Klecker B & Ipavich F M, *J Geophys Res (USA)*, 89 (1984) 8872.

19 Haland Stein, Finn Soraas & Ullaland Stein, *Geophys Res Lett (USA)*, 26 (1999) 3269.

20 Ieda A, Machida S, Mukai T, Saito Y, Yamamoto T, Nishida A, Terasawa T & Kokiban S, *J Geophys Res (USA)*, 103 (1998) 4453.

21 Machida S, Miyashita Y, Ieda A, Nishida A, Mukai T, Saito Y, Yamamato T & Kokuban S, *Geophys Res Lett (USA)*, 26 (1999) 635.